PNAS

Supporting Information for
Mechanistic insights into the regulation of cell wall hydrolysis by FtsEX and EnvC at the bacterial division site

Xin Xu, Jianwei Li, Wan-Zhen Chua, Martin A. Pages, Jian Shi, Juan A. Hermoso, Thomas G. Bernhardt, Lok-To Sham, and Min Luo

Juan A. Hermoso
Email: xjuan@iqfr.csic.es
Thomas G. Bernhardt
Email: thomas_bernhardt@hms.harvard.edu
Lok-To Sham
Email: lsham@nus.edu.sg
Min Luo
Email: dbslmin@nus.edu.sg

This PDF file includes:

Figures S1 to S18
Tables S1 to S2
Legends for Movies S1 to S2
SI References

Other supporting materials for this manuscript include the following:

Movies S1 to S2

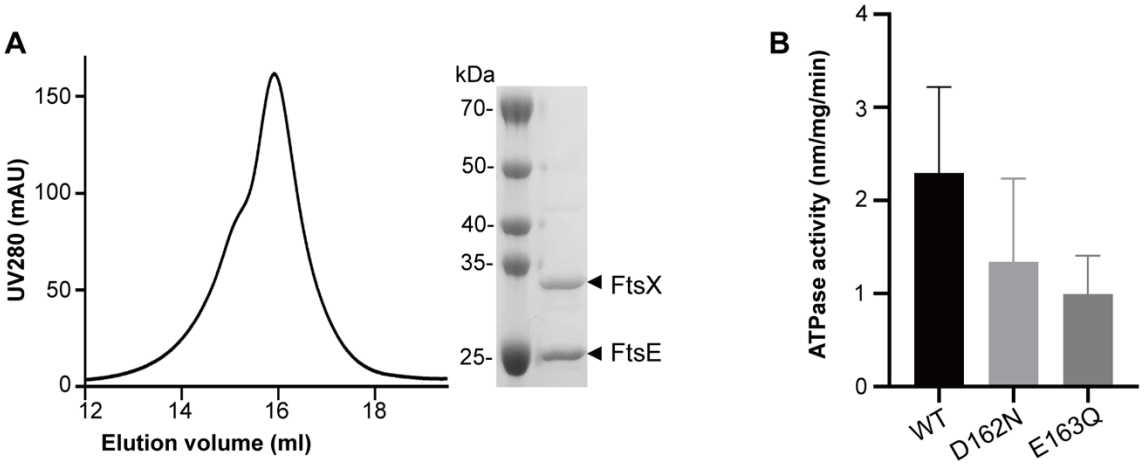

Fig. S1. Biochemical reconstitution and characterization of FtsEX complex. A. SEC profile and SDS-PAGE gel of FtsEX purified and reconstituted in peptidiscs. **B.** ATPase activity of FtsEX and its ATPase mutants (D162N and E163Q) determined. The mutants cannot bind or hydrolyze ATP. FtsEX and its mutants exhibit similar ATPase activity.

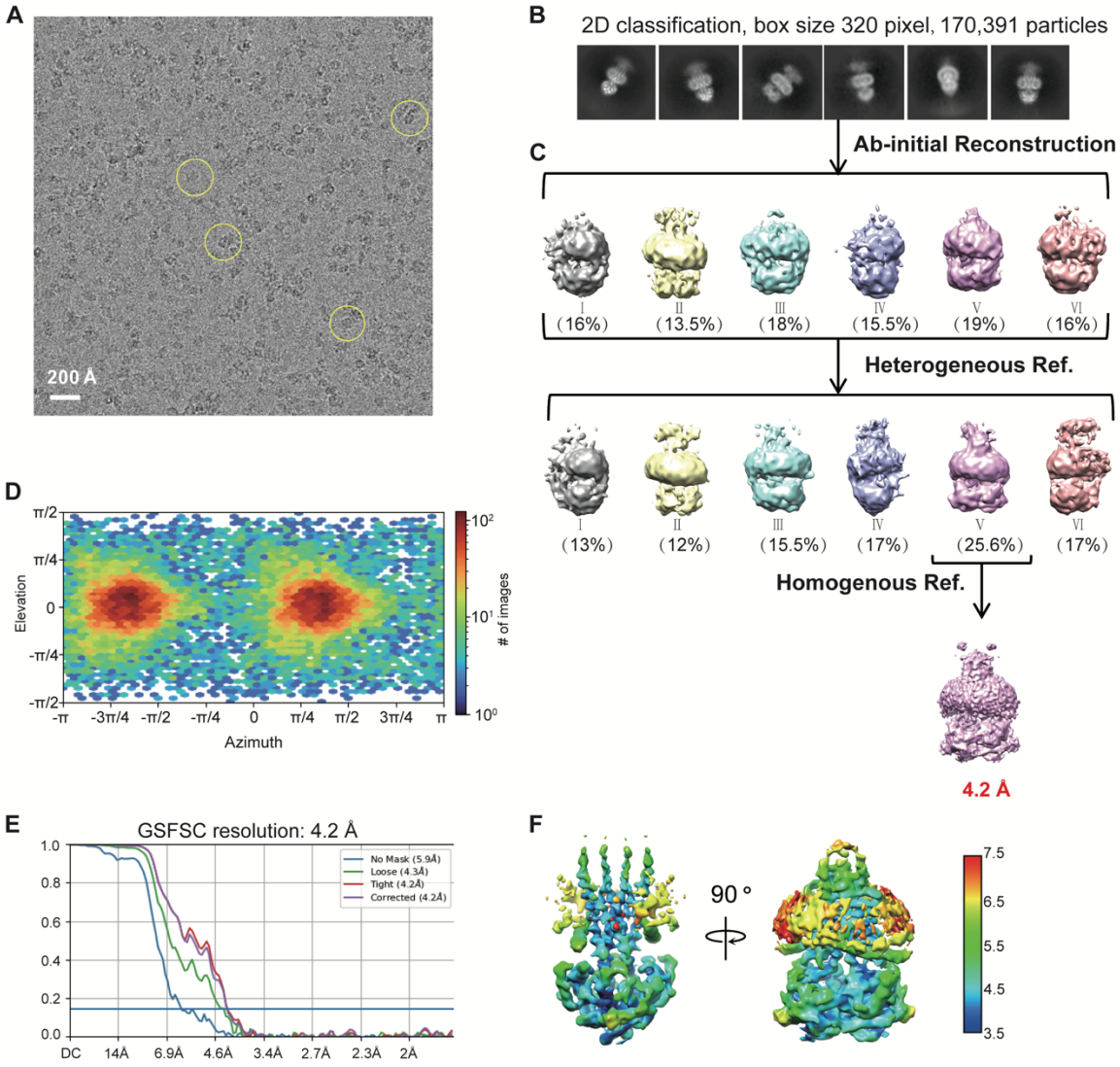

Fig. S2. Single-particle cryo-EM analysis of WT FtsEX. A. Representative cryo-EM image with several particles marked by circles. **B.** 2D averages of cryo-EM particle images. The box dimension is 270 Å. **C.** Image processing flowchart. The final maps of one major conformation with its overall resolutions is indicated in red **D.** Angular distribution of the cryo-EM particles included in the final 3D reconstruction. **E.** The Fourier shell correlation (FSC) curve: gold standard FSC between two half data maps with indicated resolution at FSC=0.143 (FSC corrected applied); **F.** The surface cryo-EM map filtered to the estimated overall resolution and colored according to local resolution.

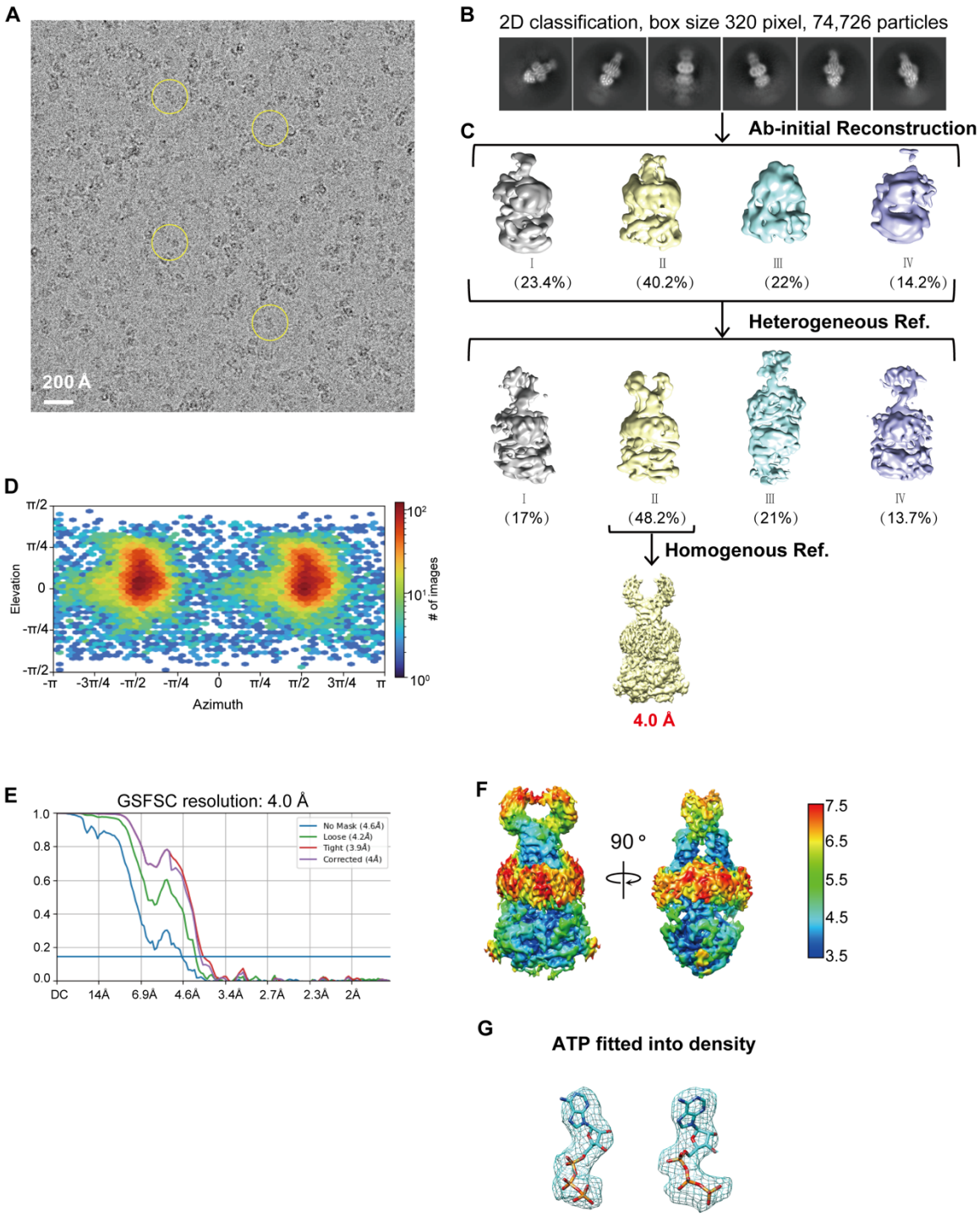

Fig. S3. Single-particle cryo-EM analysis of FtsE^{E163Q}X-ATP. A. Representative cryo-EM image with several particles marked by circles. **B.** 2D averages of cryo-EM particle images. The box dimension is 270 Å. **C.** Image processing flowchart. The final maps of one major conformation with its overall resolutions is indicated in red **D.** Angular distribution of the cryo-EM particles included in the final 3D reconstruction. **E.** The Fourier shell correlation (FSC) curve: gold-standard FSC between two half data maps with indicated resolution at FSC=0.143 (FSC corrected applied); **F.** Surface cryo-EM map filtered to the estimated overall resolution and colored according to local resolution. G. Cryo-EM density of bound ATP molecules. The ATP molecules are depicted in cartoon representation, while the EM density is represented by mesh.

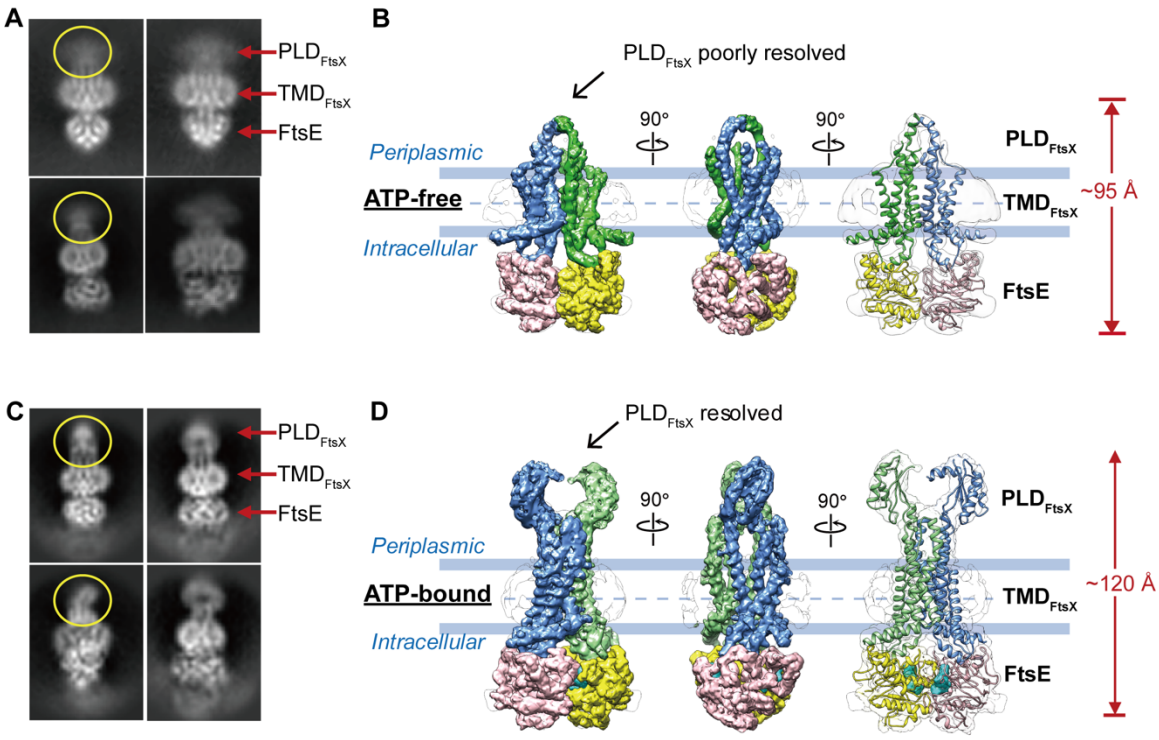

Fig. S4. Structural studies of FtsEX/EnvC complex in the presence and absence of ATP. A. 2D averages of WT FtsEX complex particles. **B.** Front- and side-views of the cryo-EM density map of WT FtsEX in the absence of ATP (left and middle), and the ribbon representation of WT FtsEX. **C.** 2D averages of ATP-bound FtsE^{E163Q}X particles. **D.** Front- and side-views of the cryo-EM density map of FtsE^{E163Q}X mutant in the presence of ATP (left and middle), and the ribbon representation of ATP-bound complex with the bound ATP density in cyan surface. Color scheme: FtsE monomers are colored in yellow and pink, FtsX monomers are colored in light green and blue.

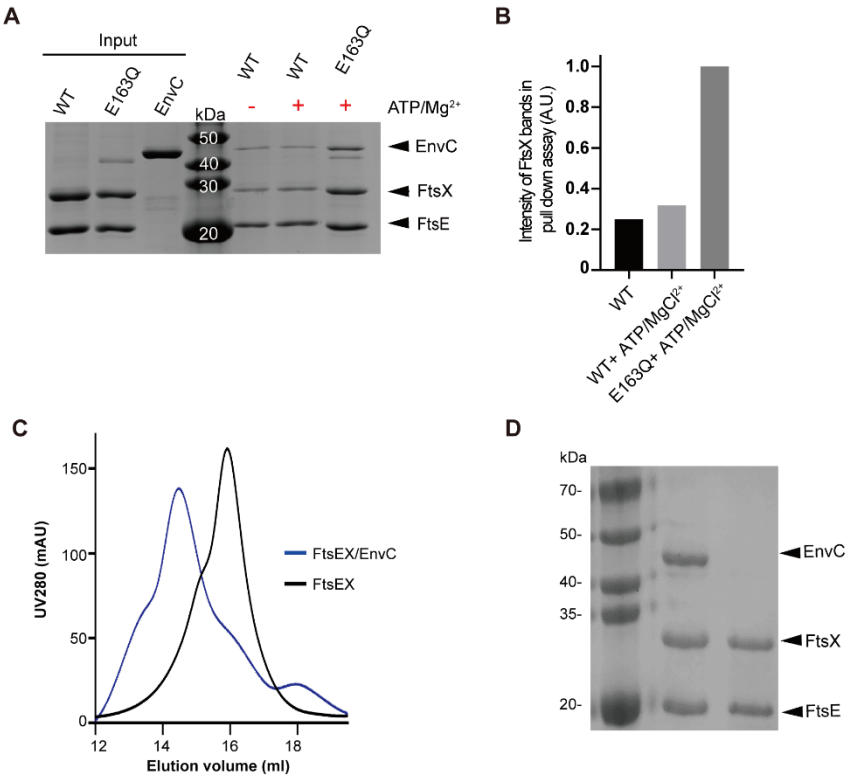

Fig. S5. Biochemical reconstitution of FtsEX/EnvC complex. A. Pull-down study of EnvC binding to FtsEX or its ATPase deficient mutant (E163Q) in the presence or absence of ATP. **B.** Quantification of FtsX retention in the pull-down assay. Most of the protein is retained in the ATP-binding state in the FtsE^{E163Q}X mutant. The intensity of the FtsX bands in the pull-down assay S5A is analyzed using ImageJ and GraphPad. **C.** SEC profiles of purified FtsEX and FtsEX/EnvC complexes reconstituted in peptidiscs. **D.** SDS-PAGE gel of purified FtsEX and FtsEX/EnvC complexes.

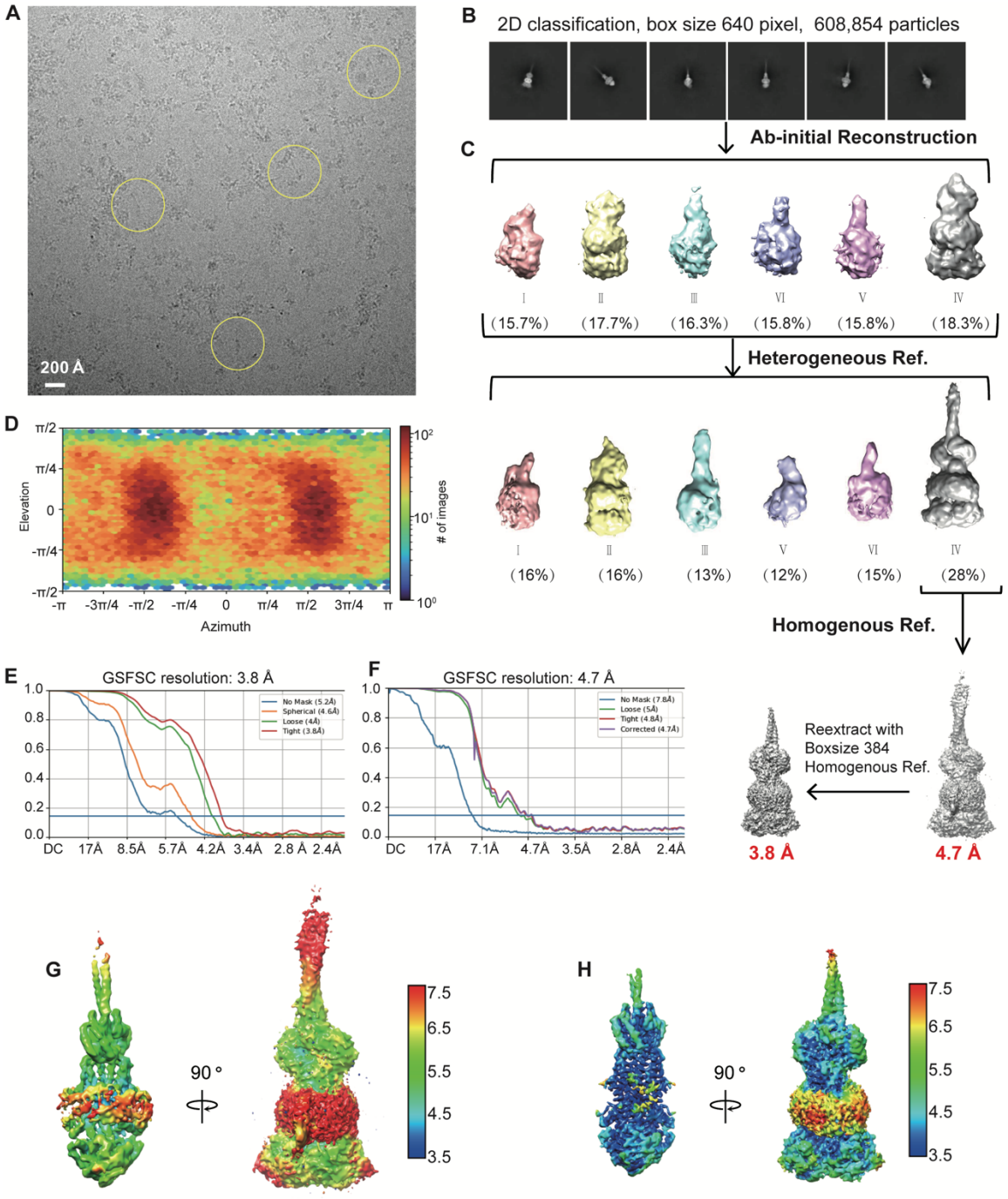

Fig. S6. Single-particle cryo-EM analysis of WT FtsEX/EnvC in the absence of ATP. A. Representative cryo-EM image with several particles marked by circles. **B.** 2D averages of cryo-EM particle images. The box dimension is 700 Å. **C.** Image processing flowchart. The final maps of one major conformation with its overall resolutions is indicated in red **D.** Angular distribution of the cryo-EM particles included in the final 3D reconstruction. **E/F.** The Fourier shell correlation (FSC) curve: gold standard FSC between two half data maps with indicated resolution at FSC=0.143 (Tight mask applied); **G/H.** The surface cryo-EM map filtered to the estimated overall resolution and colored according to local resolution.

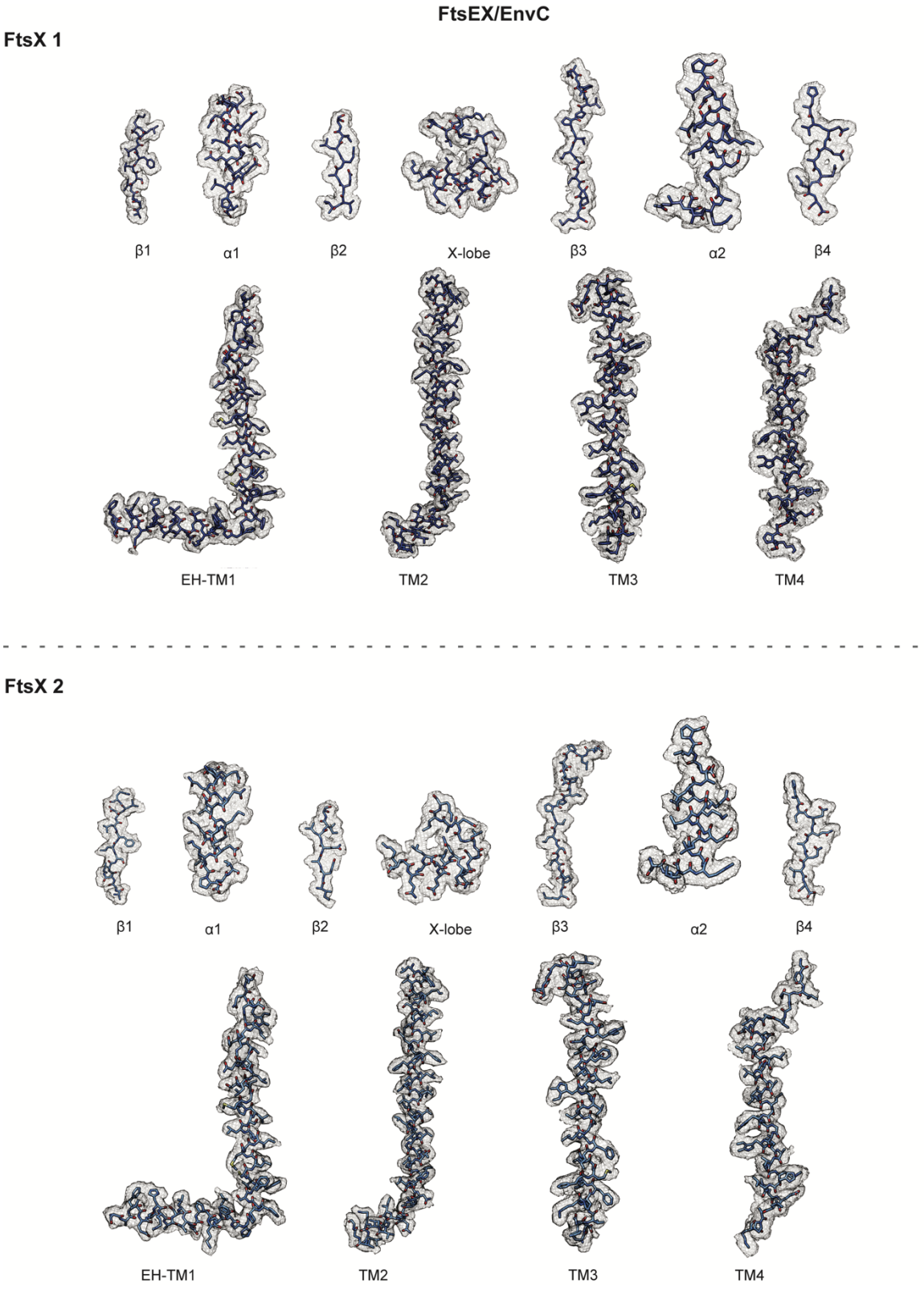

Fig. S7. Cryo-EM density of different regions of FtsX in the structure of FtsEX/EnvC complex.

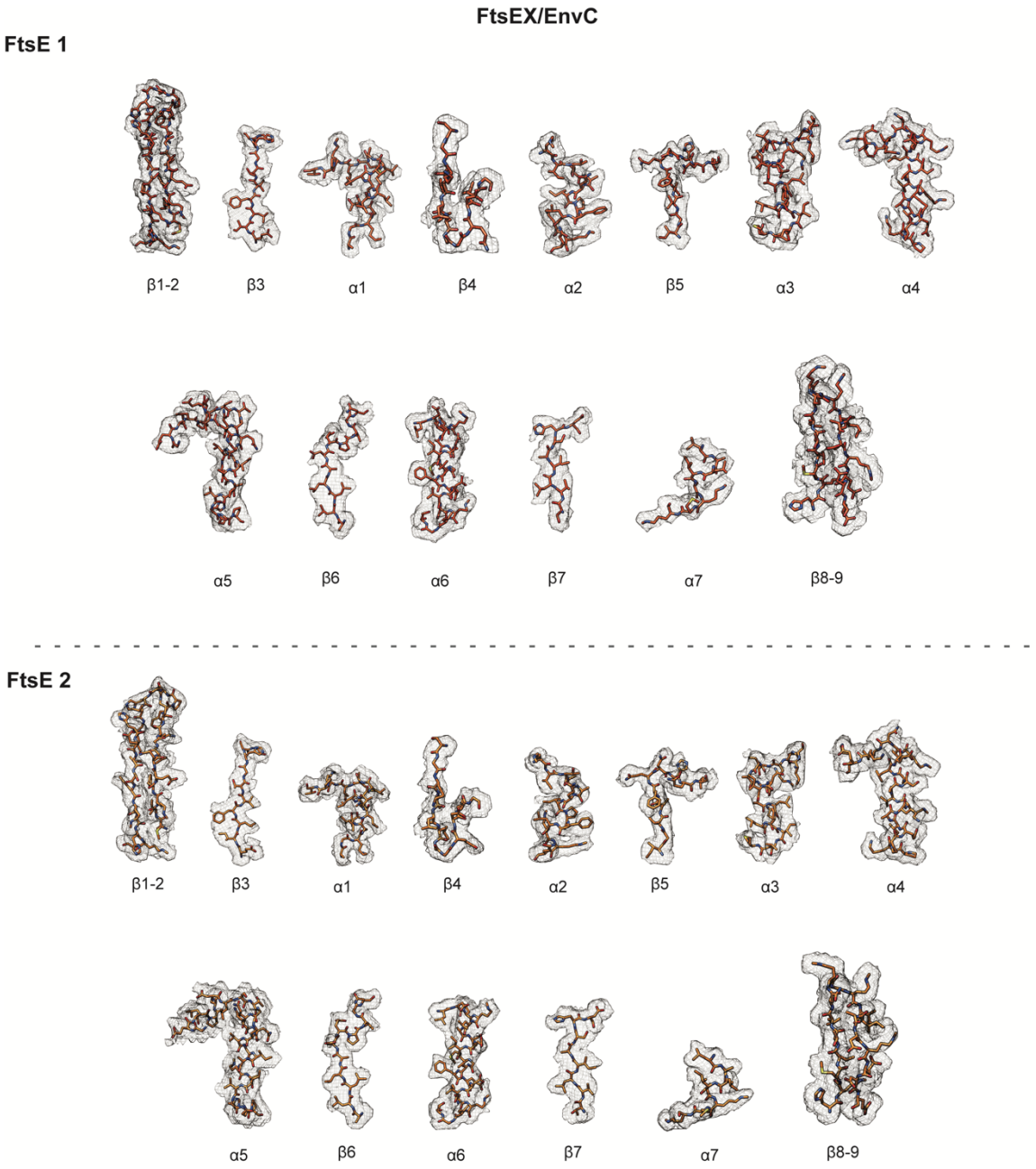

Fig. S8. Cryo-EM density of different regions of FtsE in the complex of FtsEX/EnvC.

Fig. S9. Cryo-EM density of EnvC in the complex of FtsEX/EnvC.

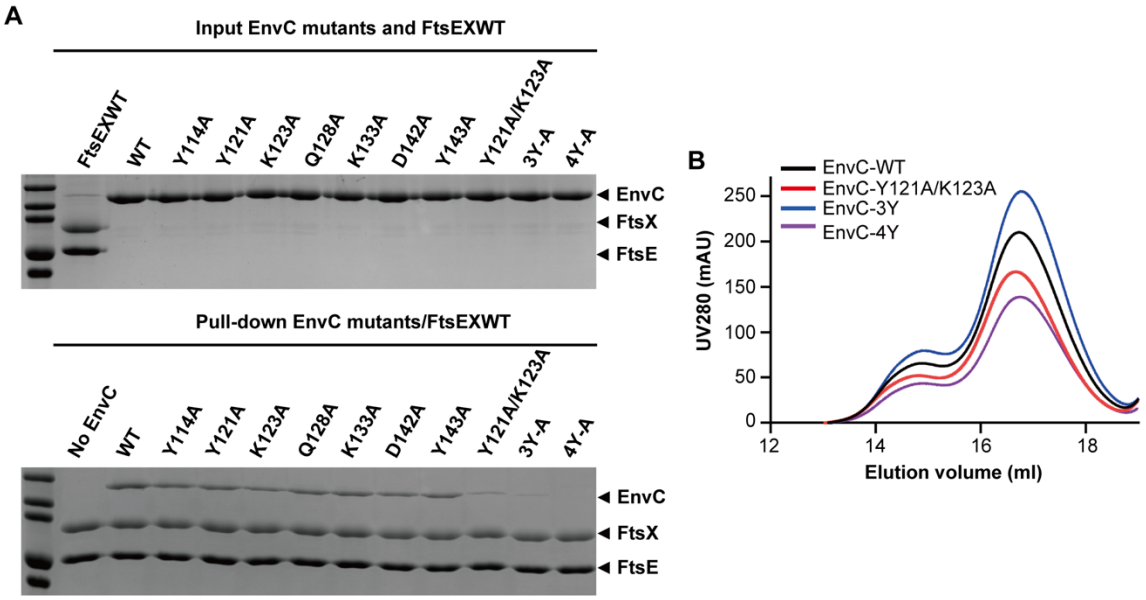

Fig. S10. Interaction study of various EnvC mutants with FtsEX. **A.** Pull-down assay of FtsEX with various EnvC mutants where FtsX-interacting residues have been mutated. "3Y-A" refers to the mutant of Y140A/Y141A/Y143A, and "4Y-A" refers to the mutant of Y114A/Y140A/Y141A/Y143A. **B.** The SEC profiles of the three EnvC mutants showed largely reduced interaction with FtsEX, as compared to the wild-type (WT) EnvC. However, the SEC profile of the mutants was similar to that of the WT, indicating that there were no issues with protein folding.

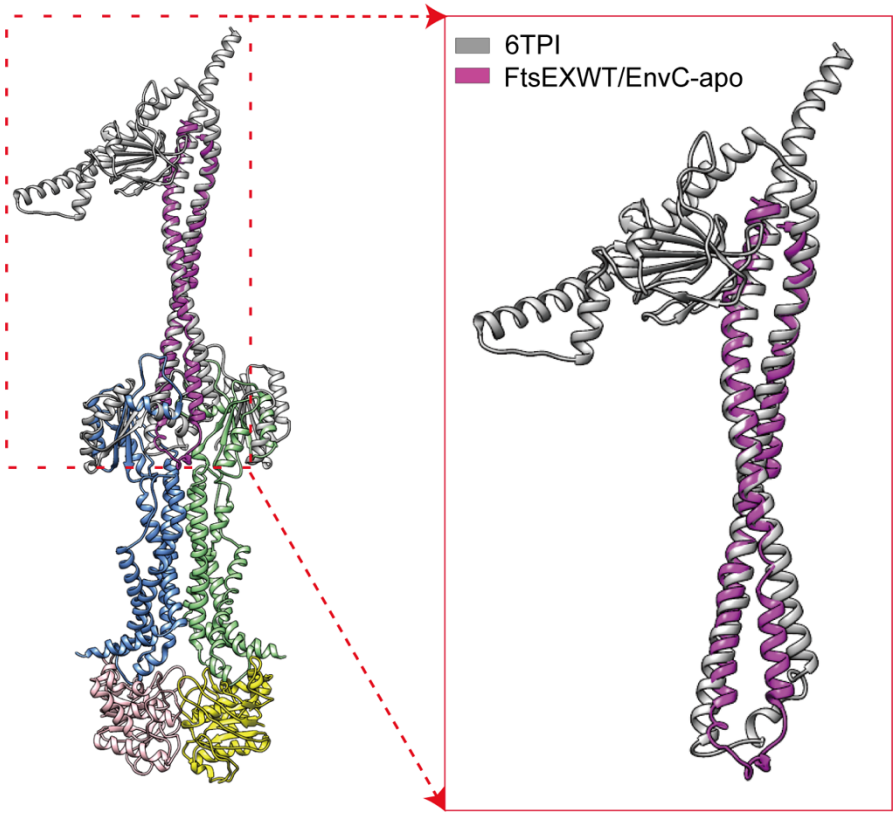

Fig. S11. Superposition of the EnvC structure from the FtsEX/EnvC complex with the EnvC-PLD crystal structure, in which EnvC adopts an autoinhibited conformation (PDB code: 6TPI) (1).

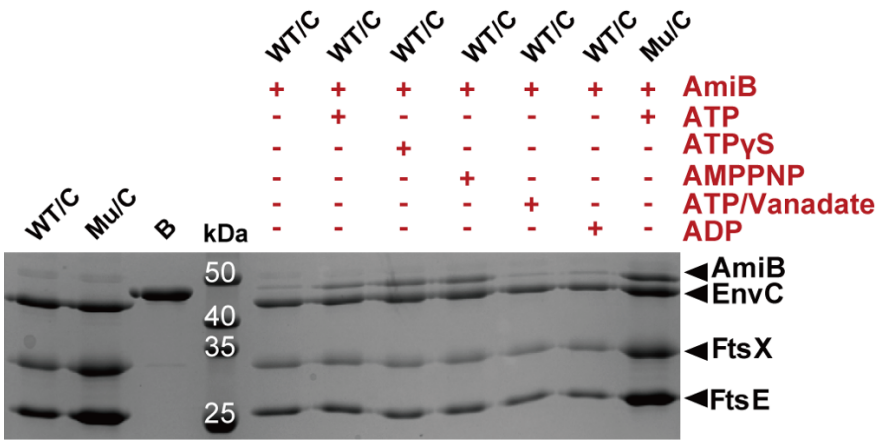

Fig. S12. Pull-down assay between AmiB and the wild-type (WT) FtsEX/EnvC complex or its mutant (Mu) of FtsE^{E163Q}X/EnvC in the presence of ATP or various ATP analogs. When FtsEX is trapped in an ATP binding (prehydrolysis) state by ATP or ATP analogs of ATPγS and AMPPNP, AmiB interaction is strong. In contrast, when FtsEX is in a post-hydrolysis state, as mimicked by ATP-Vanadate and ADP, the interaction with AmiB is relatively weak. The mutant of FtsE^{E163Q}X/EnvC in the presence of ATP showed strongest binding of AmiB. The following abbreviations are used: WT for wild-type, Mu for FtsE^{E163Q}X mutant, B for AmiB, and C for EnvC.

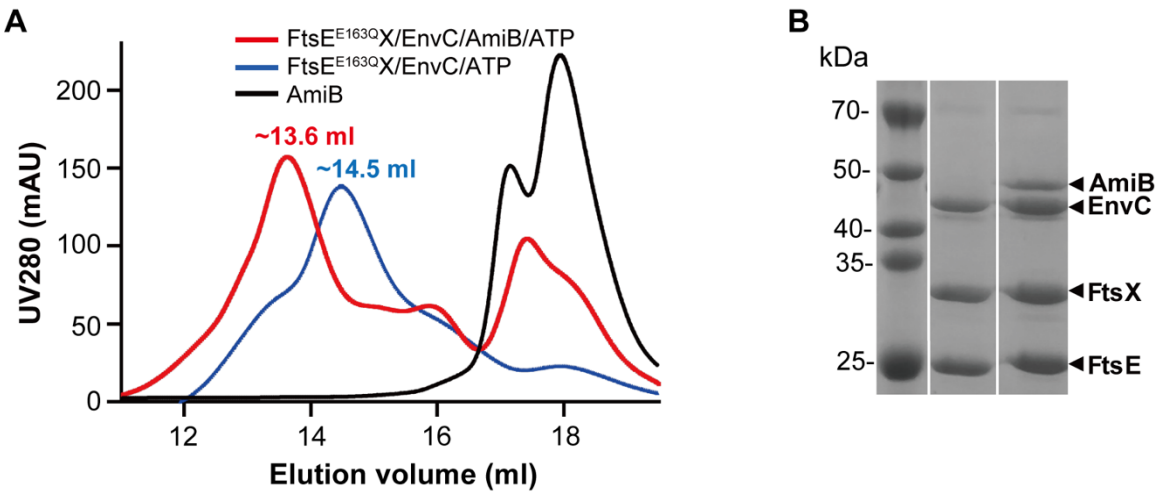

Fig. S13. Biochemical reconstitution of FtsE^{E163Q}X/EnvC/AmiB complex in the presence of ATP. A, The SEC profiles of input FtsE^{E163Q}X/EnvC (blue) and AmiB (black) proteins are shown alongside the reconstituted supercomplex of FtsE^{E163Q}X/EnvC/AmiB (red), which exhibits a peak shift relative to the FtsE^{E163Q}X/EnvC complex. All FtsEX proteins used in this study were reconstituted in peptidisc. **B.** A representative SDS-PAGE gel of the complexes, demonstrating the purity of the FtsE^{E163Q}X/EnvC input and reconstituted FtsE^{E163Q}X/EnvC/AmiB complex in peptidisc. These corresponding lanes were selected from the highest peak fraction and were cut from the same gel. They are separated with white space for clarity.

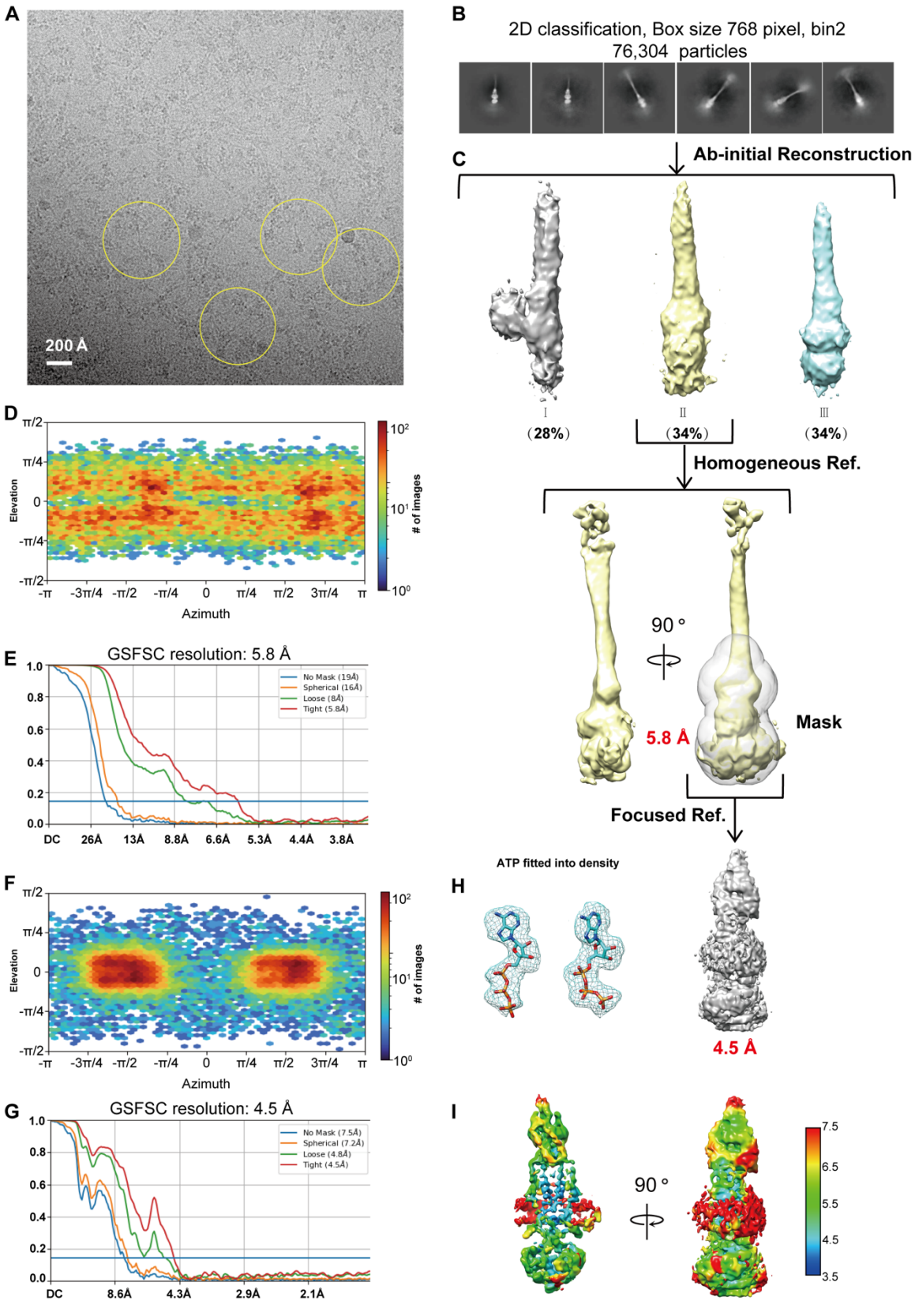
A
200 Å
B
2D classification, Box size 768 pixel, bin2
76,304 particles
C
Ab-initial Reconstruction
I
II
III
(28%)
(34%)
(34%)
Homogeneous Ref.
90 °
5.8 Å
Mask
Focused Ref.
D
Elevation
Azimuth
# of images
E
GSFSC resolution: 5.8 Å
No Mask (19Å)
Spherical (16Å)
Loose (8Å)
Tight (5.8Å)
F
G
GSFSC resolution: 4.5 Å
No Mask (7.5Å)
Spherical (7.2Å)
Loose (4.8Å)
Tight (4.5Å)
H
ATP fitted into density
4.5 Å
I
90 °

Fig. S14. Single-particle cryo-EM analysis of ATP-bound FtsE^{E163Q}X/EnvC/AmiB. A. Representative cryo-EM image with several particles marked by circles. **B.** 2D averages of cryo-EM particle images. The box dimension is 650 Å. **C.** Image processing flowchart. The final maps of one major conformation with its overall resolutions is indicated in red **D.** Angular distribution of the cryo-EM particles included in the final 3D reconstruction. **E.** The Fourier shell correlation (FSC) curve of FtsE^{E163Q}X/EnvC/AmiB-ATP: gold-standard FSC between two half data maps with indicated resolution at FSC=0.143. **F.** Angular distribution of the cryo-EM particles included in the final 3D reconstruction of FtsE^{E163Q}X/EnvC/AmiB-ATP with focused refinement using small box. **G.** The Fourier shell correlation (FSC) curve of FtsE^{E163Q}X/EnvC/AmiB-ATP with focused refinement using smaller box: gold-standard FSC between two half data maps with indicated resolution at FSC=0.143 (Tight mask applied). **H.** Cryo-EM density of the bound ATP molecules. EM density is shown in mesh, ATP structure is represented in cartoon. **I.** FtsE^{E163Q}X/EnvC/AmiB-ATP map with smaller box size. The surface cryo-EM map filtered to the estimated overall resolution and colored according to local resolution.

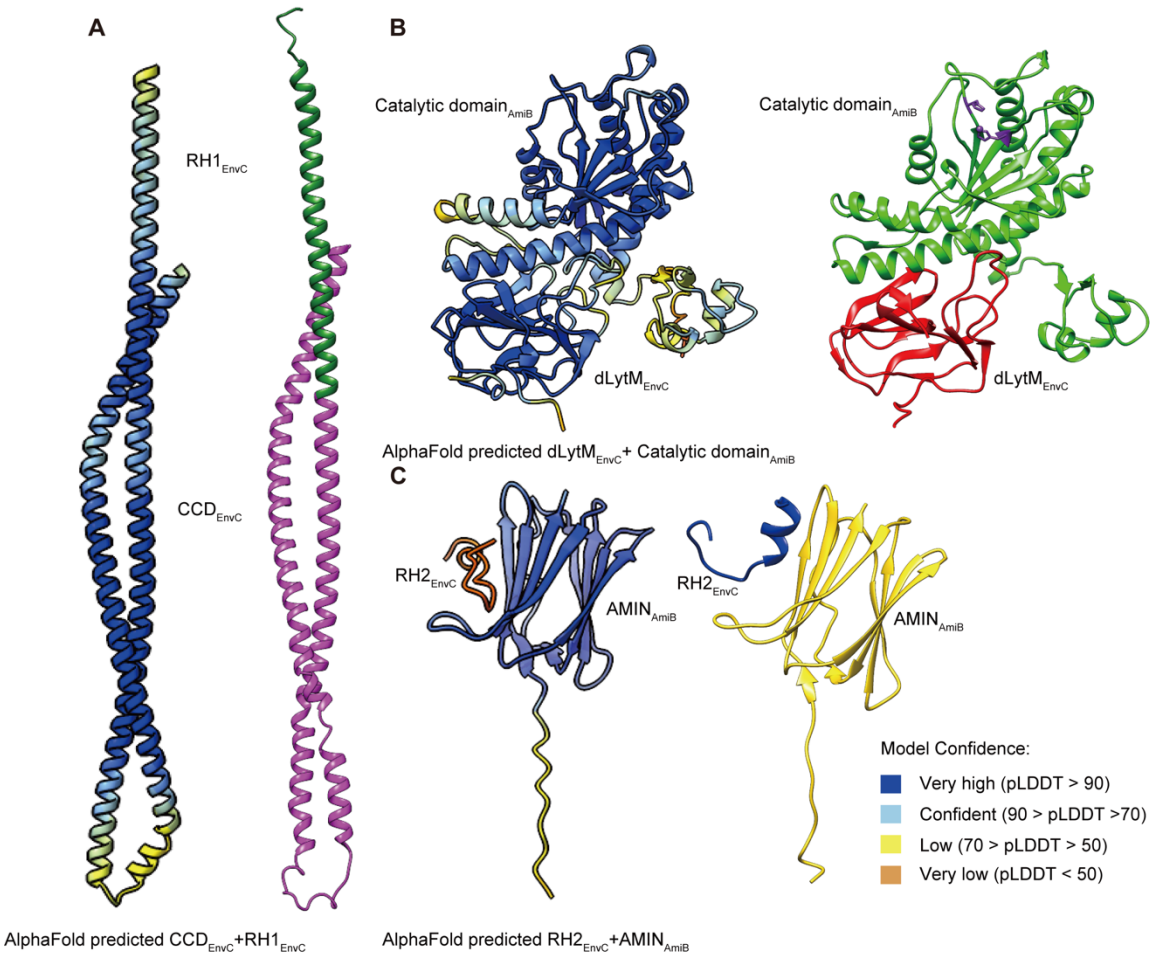

Fig. S15. AlphaFold predicted models of the CCD domain of EnvC and the interactions between activated EnvC and AimB were used in this study. **A.** The left panel shows the AlphaFold model of the CCD domain of EnvC, with confidence shown in different colors. The right panel shows the final model after rough refinement into EM density map. **B.** The left panel shows the AlphaFold model of the interaction between $dLytM_{EnvC}$ and the catalytic domain of AimB, with confidence shown in different colors. The right panel shows the final model after rough refinement into EM density map. **C.** The left panel shows the AlphaFold model of the interaction between $RH2_{EnvC}$ and the AMIN domain of AimB, with confidence shown in different colors. The right panel shows the final model after rough refinement with EM density map.

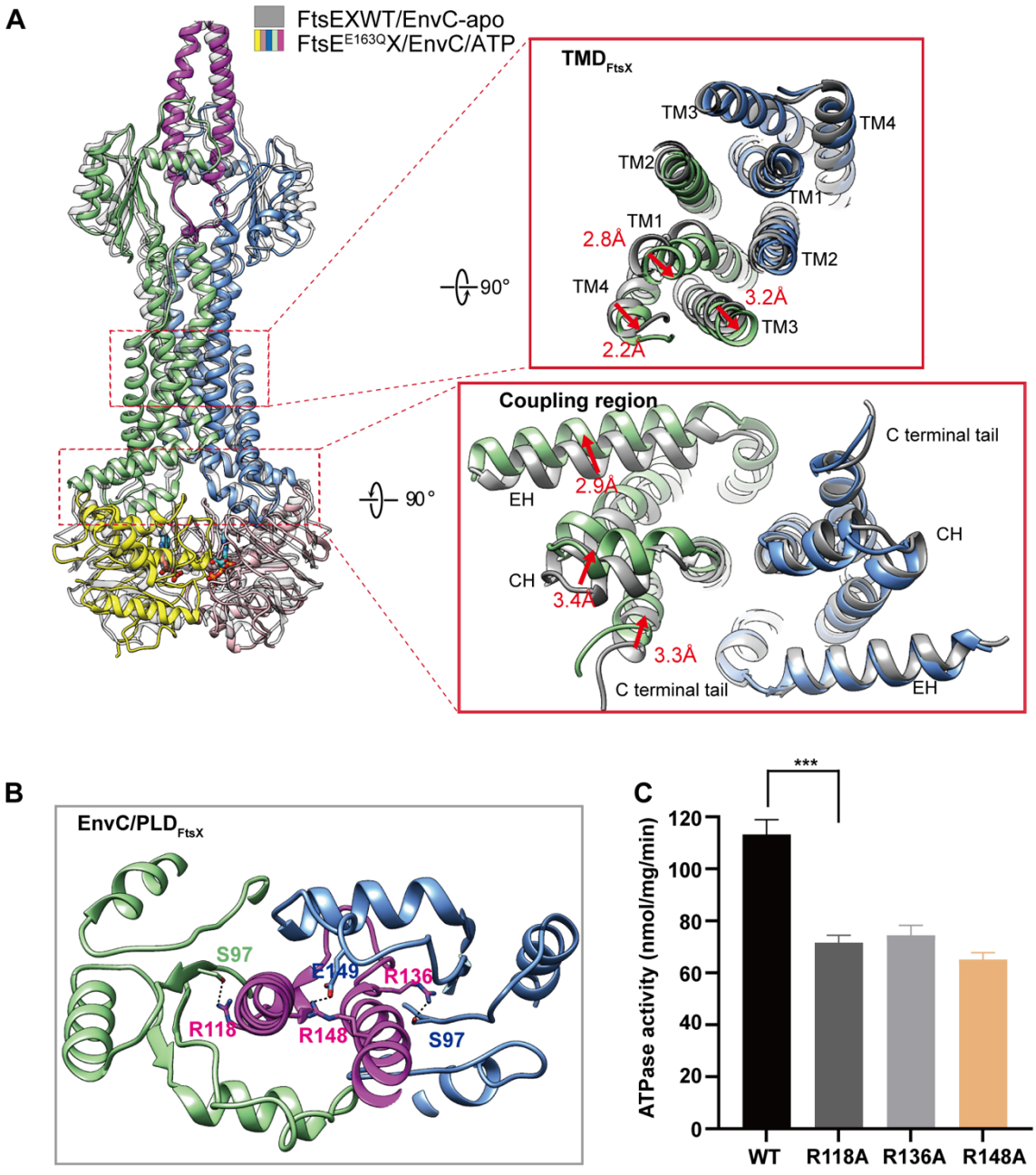

Fig. S16. **ATP binding at FtsE induces conformational changes that are transferred to EnvC through FtsX coupling helix and transmembrane domain (TMD). A.** The left panel shows an overlay of the ATP-bound FtsE^{E163Q}X/EnvC complex (colored by subunits) with the apo FtsEX/EnvC structure (colored in gray). The upper right panel zooms in on the TMD domain, highlighting the conformational changes induced by ATP binding. The bottom right panel zooms in on the coupling helices (CH) region. **B.** The ATP binding induced new interactions between FtsX and EnvC are shown. **C.** Mutations of residues involved in the new interactions between FtsX and EnvC showed only minor inhibition of the ATPase activity of FtsEX.

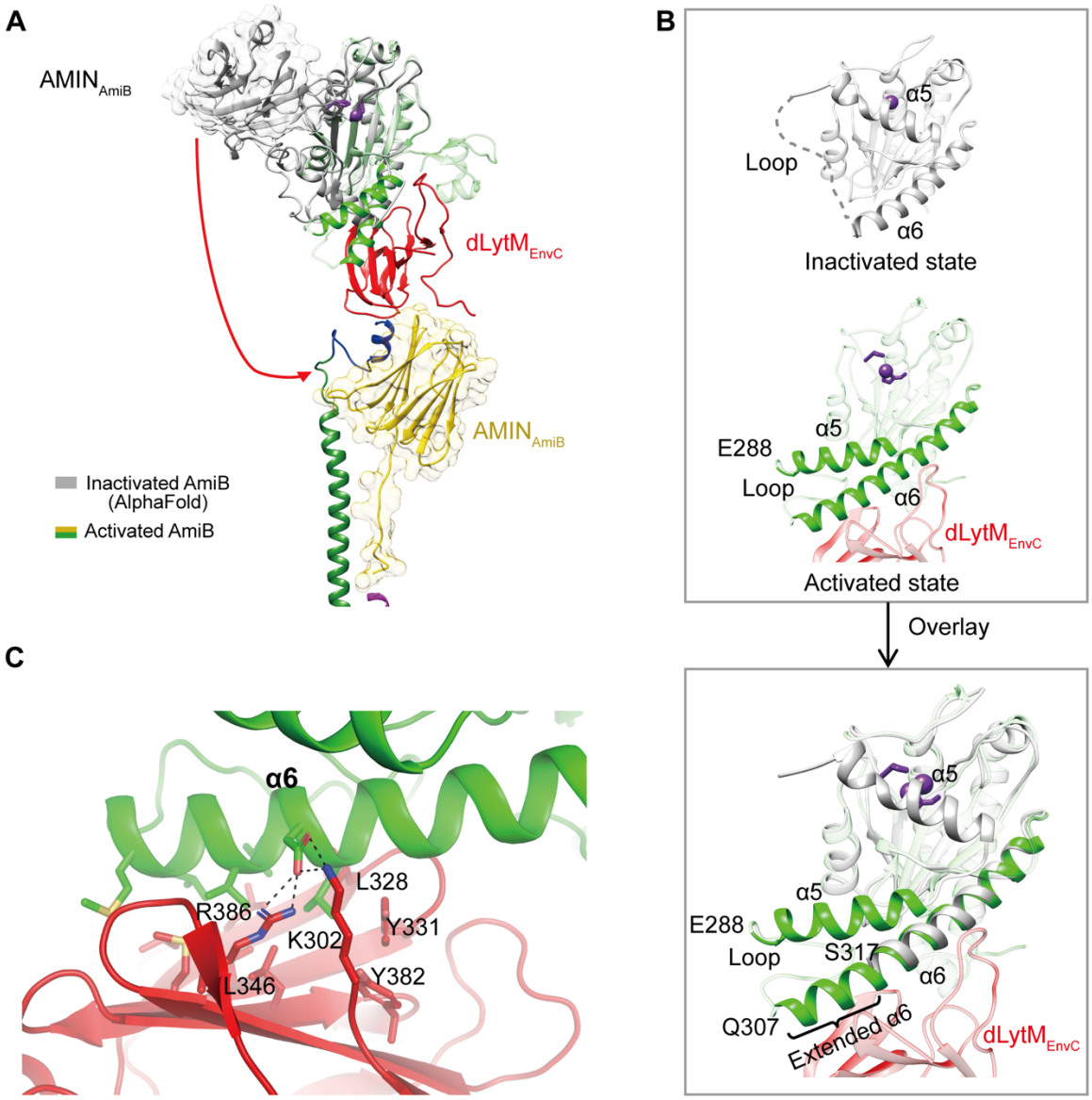

Fig. S17. Conformational changes leading to AmiB activation. A. The relocation of AMIN$_{AmiB}$ upon activation. The left panel displays the comparison between predicted inactivated state of AmiB (colored in gray) and the activated state in the supercomplex (colored by different domains) with the catalytic domain docked on each other. **B.** The upper panel shows the predicted structure of the catalytic domain of inactivated AmiB (colored in grey) and the activated AmiB upon interaction with EnvC. The AlphaFold model of AmiB is similar to the crystal structure of inactivated AmiC (PDB code: 4BIN) (2). In the activated state, the helical structure of α6 is extended and the regulatory α5 helix moves away, exposing the active site. The bottom panel displays an overlay of the inactivated and activated catalytic domains of AmiB. **C.** The detailed interaction between the α6 helix of AmiB's catalytic domain and the dLytM domain of EnvC, as predicted by AlphaFold. The color scheme used in this figure is as follows: the inactivated state of AmiB is colored in gray, the AMIN domain of the activated AmiB is colored in yellow, the catalytic domain of the activated AmiB is colored in green, with catalytic residues and Zn^{2+} colored in purple, and the interacting dLytM domain of EnvC is coloured in red.

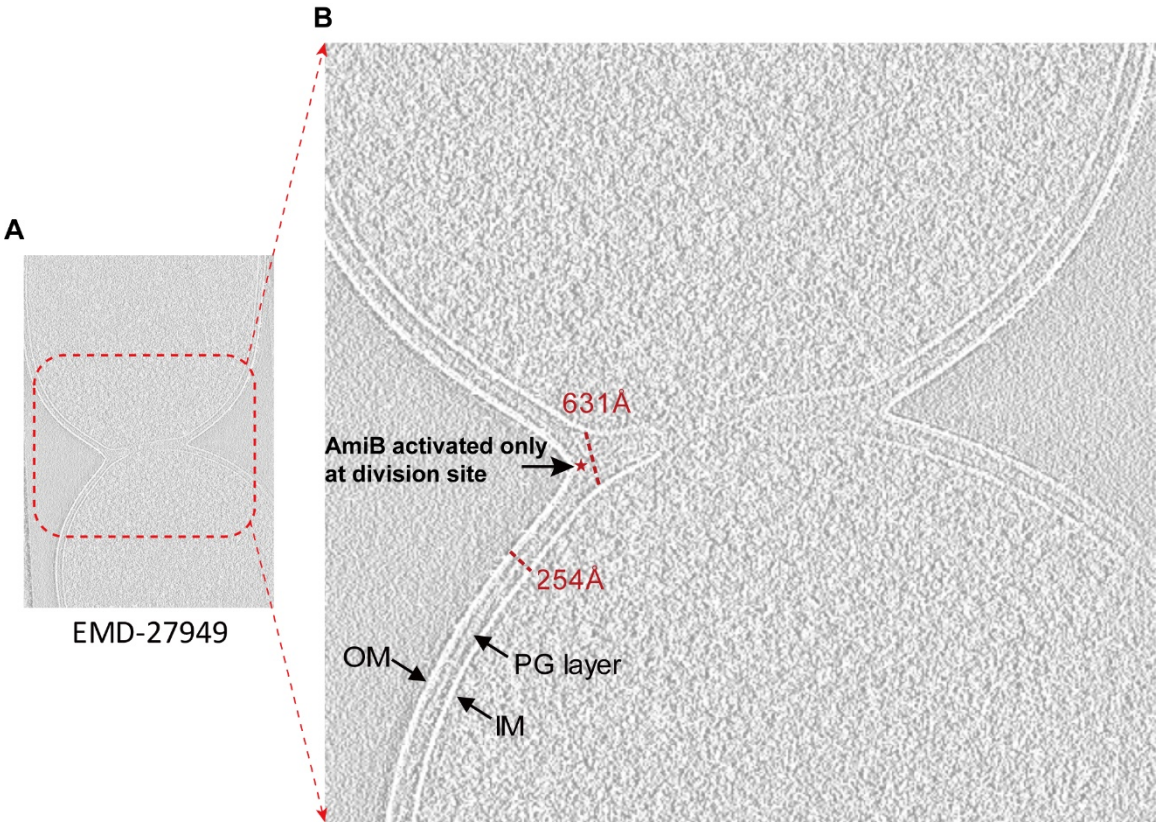

Fig. S18. The thickness of PG in division cell suggesting activated supercomplex of FtsEX/EnvC/AmiB only function in the division site. A. Tomogram image of *E. coli* in a division state (EMD-27949) (3). **B.** The thickness between OM and IM in different sites of division cell have dramatic differences(~630 Å at division site and ~250 Å at side wall). This indicated that activated FtsEX-EnvC-AmiB complex which has an extended size (full size ~380 Å) can only function normally at the division site. OM, outer membrane; IM, inner membrane. PG layer is located between OM and IM. The location of the proposed cleavage site is denoted by a star symbol.

Table S1. Statistics of the cryo-EM structures presented in this study

Cryo-EM data collection and processing	FtsEX(WT) (EMDB-35203, PDB 8I6Q)	$FtsE^{E163Q}$X-ATP (EMDB-35204, PDB 8I6R)	FtsEX /EnvC(WT) (EMDB-35201, PDB 8I6O)	$FtsE^{E163Q}$X/EnvC/AmiB-ATP	
				focused map (EMDB 35205, PDB 8I6S)	full map (EMDB-35213)
Voltage(kV)	300	300	300	300	
Electron dose ($e^-/Å^2$)	50	47	55	47	
Physical pixel (Å)	0.858	0.858	1.105	0.858	
Number of movies	5547	4756	8810	6670	
Number of particles for final map	28,977	27,049	175,354	35,887	37,628
Resolution (Å)	4.2	4.0	3.8	4.5	5.8
Map B-factor ($Å^2$)	-170	-138	-134	-131	-216
Model refinement					
Number of protein residues	809	1196	1196	1125	--
Number of chains	4	4	5	5	--
Number of atoms	3970	7733	9053	8598	--
Ligands	--	2 ATP	--	2 ATP	--
Geometric parameters (r.m.s.d.)					
Bond length (Å)	0.001	0.005	0.005	0.005	--
Bond angle (º)	0.335	1.200	0.848	0.738	--
Ramachandran statistics					
Residues favoured (%)	98.10	90.29	96.29	97.84	--
Residues allowed (%)	1.77	7.21	3.71	2.07	--
Residues disallowed (%)	0.13	2.5	0.00	0.09	--
Rotamer outliers (%)	0.00	2.50	1.54	2.71	--
MolProbity Score	1.41	3.29	2.08	1.68	--

Table S2. Oligonucleotides used in this study

Primer	Sequence (5'-3')	template
For construction of His_6- FtsEX		
EX F	CCCCTCTAGATTTAAGAAGGAGATATACATATGATCC GCTTCGAGCAGGTCGGCAAACGC	Genome of *Pseudomonas aeruginosa*
EX R	CCGCAAGCTTTCAGCGCGGCGCCAGCTCGCGCA GGTGGCGGGCC	
For construction of His_6-SUMO-EnvC		
EnvC F	TTGGTGGATCCGACGAGCGCGCCGACACCCAAC	Genome of *Pseudomonas aeruginosa*
EnvC R	TCGACAAGCTTCTATCCCTGTGCGCGGCACCAGG	
For construction of His_6-SUMO-EnvC		
AmiB F	GGTGGTACCGCGCAAATCAAGAGCGTGCG	Genome of *Pseudomonas aeruginosa*
AmiB R	GGATCCTTATTACTGGGCCGCCAGGGCGGTGCTC GGGATGGACAG	
For FtsE and EnvC mutations		
FtsE D162N F	CTGCTGGCGAACGAACCCACCGGCAACCTCGA	FtsEXWT
FtsE D162N R	GGTGGGTTCGTTCGCCAGCAGCAGGGCCGGCT	
FtsE E163Q F	CTGGCGGACCAACCCACCGGCAACCTCGACC	FtsEXWT
FtsE E163Q R	GCCGGTGGGTTGGTCCGCCAGCAGCAGGGCCG	
EnvC Y114A F	CGCGCGGCCGCCCAGAGTGGACGCGAGGAAT	EnvCWT
EnvC Y114A R	TCCACTCTGGGCGGCCGCGCGGGCCTGGATG	
EnvC R118A F	CCAGAGTGGAGCCGAGGAATACCTGAAGCTGC	EnvCWT
EnvC R118A R	GGTATTCCTCGGCTCCACTCTGGTAGGCCGCG	
EnvC Y121A F	CGCGAGGAAGCCCTGAAGCTGCTGCTGAACC	EnvCWT
EnvC Y121A R	CAGCTTCAGGGCTTCCTCGCGTCCACTCTGG	
EnvC K123A F	GGAATACCTGGCGCTGCTGCTGAACCAGGAAC	EnvCWT
EnvC K123A R	TCAGCAGCAGCGCCAGGTATTCCTCGCGTCCA	
EnvC Q128A F	GCTGCTGAACGCGGAACACCCGGAAAAATTCA	EnvCWT
EnvC Q128A R	CCGGGTGTTCCGCGTTCAGCAGCAGCTTCAGG	
EnvC K133A F	ACACCCGGAAGCATTCAGCCGCACCCTCACCT	EnvCWT
EnvC K133A R	TGCGGCTGAATGCTTCCGGGTGTTCCTGGTTC	
EnvC R136A F	AAAATTCAGCGCCACCCTCACCTACTACGACT	EnvCWT
EnvC R136A R	AGGTGAGGGTGGCGCTGAATTTTTCCGGGTGT	
EnvC D142A F	ACCTACTACGCCTACATCAACAAAGCCCGTCTC	EnvCWT
EnvC D142A R	GTTGATGTAGGCGTAGTAGGTGAGGGTGCGGCT	
EnvC Y143A F	CTACTACGACGCCATCAACAAAGCCCGTCTCG	EnvCWT
EnvC Y143A R	CTTTGTTGATGGCGTCGTAGTAGGTGAGGGTG	
EnvC R148A F	CAACAAAGCCGCTCTCGAACAGCTCGCCAGCT	EnvCWT
EnvC R148A R	GCTGTTCGAGAGCGGCTTTGTTGATGTAGTCG	
EnvC Y121A/K123A F	AGGAAGCCCTGGCGCTGCTGCTGAACCAGGAAC	EnvCWT
EnvC Y121A/K123A R	AGCAGCGCCAGGGCTTCCTCGCGTCCACTCTGGT A	
EnvC 3Y-A F	GCCGCCGACGCCATCAACAAAGCCCGTCTCGAAC AG	EnvCWT
EnvC 3Y-A R	GTTGATGGCGTCGGCGGCGGTGAGGGTGCGGCT GAAT	
EnvC 4Y-A F	GCCGCCGACGCCATCAACAAAGCCCGTCTCGAAC AG	EnvC 3Y-A
EnvC4Y-A R	GTTGATGGCGTCGGCGGCGGTGAGGGTGCGGCT GAAT	

Movie S1 (separate file). ATP binding leading to PLD restraining.

Movie S2 (separate file). EnvC activation caused by the restraining of PLD upon ATP binding.

SI References

1. J. Cook *et al.*, Insights into bacterial cell division from a structure of EnvC bound to the FtsX periplasmic domain. *Proc Natl Acad Sci U S A* **117**, 28355-28365 (2020).
2. M. Rocaboy *et al.*, The crystal structure of the cell division amidase AmiC reveals the fold of the AMIN domain, a new peptidoglycan binding domain. *Mol Microbiol* **90**, 267-277 (2013).
3. P. P. Navarro *et al.*, Cell wall synthesis and remodelling dynamics determine division site architecture and cell shape in Escherichia coli. *Nat Microbiol* **7**, 1621-1634 (2022).